On the constitutive behaviour of polycarbonate under large deformation

Gérard Buisson and K. Ravi-Chandar*
Department of Mechanical Engineering, University of Houston, Houston, Texas 77204, USA
(Received 17 July 1989; revised 13 November 1989; accepted 18 November 1989)

The uniaxial stress–strain behaviour of polycarbonate (Lexan) is examined. A grid technique is used to determine the inhomogeneous strain field associated with a steadily growing neck. An extension of photoelasticity is used in obtaining the stress variation along the line of symmetry in the neck. Comparing the grid and photoelastic measurements, the true-stress–stretch curve is established for polycarbonate.

(Keywords: polycarbonate; necking; true-stress–stretch measurements)

INTRODUCTION

Certain non-crosslinked polymers are capable of sustaining very large inelastic deformations before eventual failure. The micromechanism responsible for such behaviour can be described in terms of the generation of molecular orientation in the initially randomly oriented polymer. Upon breaking of secondary bonds and untangling of molecular entanglements, large strains (irreversible) are achieved. This capacity for orientation facilitates localization of deformation in or around regions of stress concentration. *Figure 1* illustrates two examples of deformation localization. In *Figure 1a*, the near-tip region of a cracked specimen is shown. The bands show regions along which large molecular orientation has occurred. *Figure 1b* shows localization of deformation under combined tension and torsion. The deformation localization occurs in annular regions on an inclined plane, as illustrated. Any attempt to model these deformation phenomena would require a knowledge of the constitutive behaviour of the material.

A simple experiment to characterize the material behaviour is the uniaxial loading experiment. In this class of materials, however, even under such homogeneous loading conditions, the deformation localizes in certain locations and introduces non-homogeneous deformation and stress fields. Under large strains, the localization eventually develops into a steadily growing 'neck'. This problem of necking has received much attention in the literature; most of the investigations, however, have been aimed at modelling the growth of the neck itself, assuming a constitutive model.

Hutchinson and Neale[1] presented a simple three-dimensional analysis for neck propagation along a cylindrical round bar. In this analysis, a J_2 flow theory of plasticity was used to characterize the inelastic stress–strain behaviour of polymers. The load required for steady-state necking was estimated in the analysis. Tugcu and Neale[2,3] carried out a finite-element analysis of necking under axisymmetric and plane strain conditions. The results presented in these different analyses were generally the computed load–elongation curves; stress and strain contours for different locations across the necked region were obtained only in the finite-element analyses. In comparing the load–elongation curves, a very small difference between the model is observed. Furthermore, the only experimental results available, so far, for comparison have been the load–elongation curves such as the one shown in *Figure 2* and some strain measures[4].

To obtain the true-stress–true-strain relationship, G'Sell and Jonas[5] used an hourglass-shaped round bar with a special diametral transducer to determine the instantaneous diameter and also to control the loading rate. The Cauchy stress was calculated as the load divided by the current cross-sectional area. The assumption that the stress field was uniform across the cross-section was justified through an estimate of the Bridgman triaxiality factor. Also, the strains were obtained from the diameter changes by assuming that the large deformations occurred at constant volume.

Before going into details of the present experiments, a qualitative description of the sequence of events unfolding in a uniaxial test is provided. When pulled in uniaxial tension, polycarbonate behaves as shown in *Figure 2*. On the curve, obtained experimentally, we observe that, for small deformations, the load–elongation curve is linear and the deformations are elastic; polycarbonate also exhibits a non-linear elastic/viscoelastic behaviour up to yielding, which corresponds to the peak load in *Figure 2*.

At the maximum load, the system reaches a shear instability and Lüder's bands appear, similar to observations in steels, but not at 45° to the load direction. Whereas this instability leads to imminent failure in the case of metals, in polymers the instability facilitates large-scale motion of the long molecules and orients them in a direction parallel to the load. If the crosshead extension is continued, the load falls below the maximum and additional displacements produce progressively greater strains, causing the unstable shear bands to stabilize into a necked profile, as shown in the insets of *Figure 2*. With the molecules oriented along the load

* To whom correspondence should be addressed

0032-3861/90/112071-06

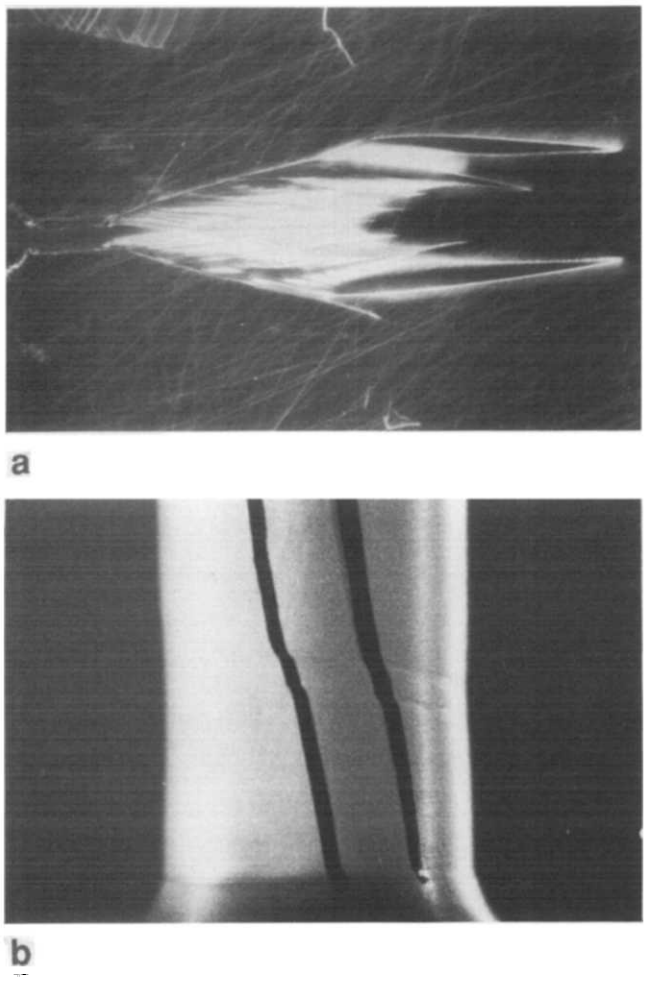

Figure 1 Deformation localizations under different modes of loading in polycarbonate

direction, the polymer is able to withstand a significant fraction of the load at instability.

Upon further crosshead extension, the neck stabilizes itself to a constant profile and travels along the specimen until all available undrawn material has been 'consumed'. During this process the load remains almost constant, as shown in *Figure 2*. This phenomenon is called *cold drawing*.

After cold drawing is complete, i.e. when the neck has propagated completely through the length of the specimen, the stress required to produce further strain increases; the load–deflection curve once again sweeps upwards. At this stage, the applied force comes up against strain limits due to covalent molecular bonds and tightened entanglements, leading to high stresses. These high stresses cannot be alleviated by strain localization in the same way as in the unoriented material, and rupture occurs.

In the present investigation, the true-stress–true-strain relationship in uniaxial tension is explored. A fine-grid technique is employed, as described in the next section, to obtain the strain field; a stress-optic technique is used to characterize the stress field. From a correlation of the two measurements, the uniaxial stress–strain relation is obtained.

EXPERIMENTAL STRAIN ANALYSIS

For the strain analysis, a grid technique was used, which consists of depositing a grid pattern on a specimen, recording this pattern before and after loading, and measuring the coordinates of each point in order to obtain the displacement field as well as the strain field all over the specimen. Note that this technique will be accurate only in the case of large strains, i.e. when the error induced in the measurement of the coordinates of any point on the grid is negligible or small compared with the displacement value at that point. In the case of small strains or displacements, it becomes much more difficult to maintain a good level of accuracy on the results owing to the increased relative error on the measurements.

A coating was deposited on the surface of the specimen by vacuum deposition of silver through a grid of 4×4 lines/mm^2. Close to the edges of the specimen, some irregularities in the grid pattern were detected, and hence measurements were not obtained along the edges. The specimen was mounted and tested in an Instron machine. The tests were all performed at a constant crosshead speed set to 2.5 mm min^{-1} in order to prevent any unexpected failure during the neck propagation from random flaws in the material.

Pictures of the undeformed grid pattern in the unloaded state and of the deformed grid under steady-state neck propagation were obtained on a digital video system, as shown in *Figure 3*. From the records of the grid in the deformed and undeformed configurations, the displacements were obtained; an origin was arbitrarily set on the deformed grid, in the region where the material was still elastic. A bicubic interpolation on the surface of displacement 'located' over the deformed grid was used to obtain the surface of displacement for the points of interest. The computation of the gradient of the displacements at any point was done using a polynomial fit on the displacement components along vertical and horizontal lines. The order of the polynomial used depended upon the variation of displacement components U_X and U_Y with respect to X and Y.

Figure 4 shows the variation of the stretches λ_1 and λ_2 along the Y axis. The stretch λ_i is the ratio of the final to initial length in the direction of the i axis and is related to the Eulerian strain components by:

$$\lambda_i = 1/(1-2\varepsilon_{ii})^{1/2} \qquad (i=1,2) \qquad \text{no sum} \qquad (1)$$

In the elastic region before the neck, λ_2 is a little bit greater than 1, meaning that the material is stretched in the loading direction, whereas λ_1 is smaller than 1 owing to the Poisson's contraction during small elastic deformation. As we go along the neck, λ_1 decreases down to 0.75, showing a larger contraction of the cross section, but λ_2 increases much more to reach a plateau at around 1.7, which is very close to the 70% stretch we measured during the test. Notice that λ_3 (principal stretch in the third direction) should be very close to λ_1 since the cross section of the specimen was square.

Figure 5 shows that all stretch components remain constant along the X direction perpendicular to the loading direction, in both the 'elastic' and 'plastic' regions.

EXPERIMENTAL STRESS ANALYSIS

In order to determine experimentally the uniaxial stress–strain relationship, it is necessary to determine the (non-homogeneous) true or Cauchy stress field during the evolution of necking. In the present study, the stress

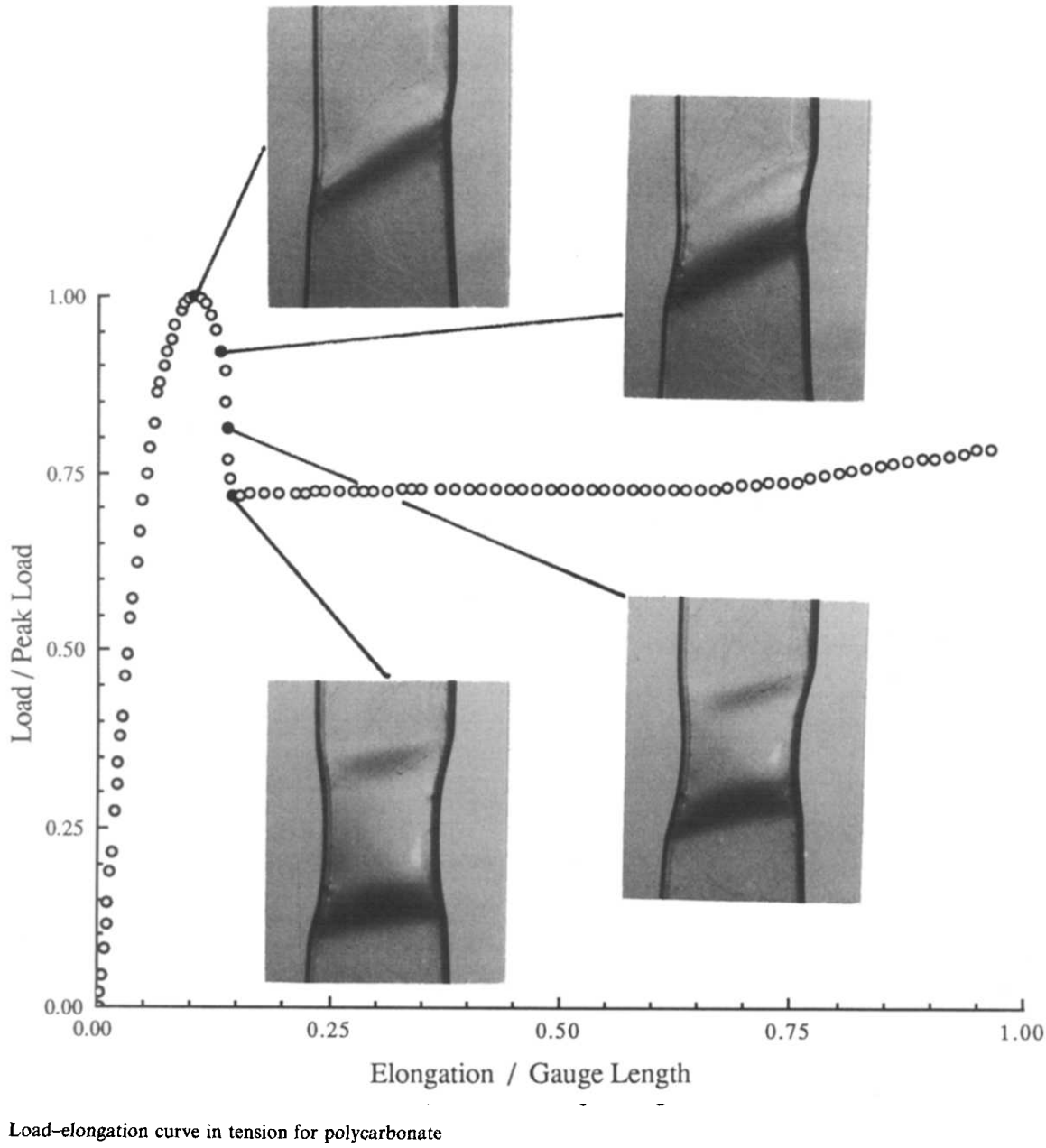

Figure 2 Load–elongation curve in tension for polycarbonate

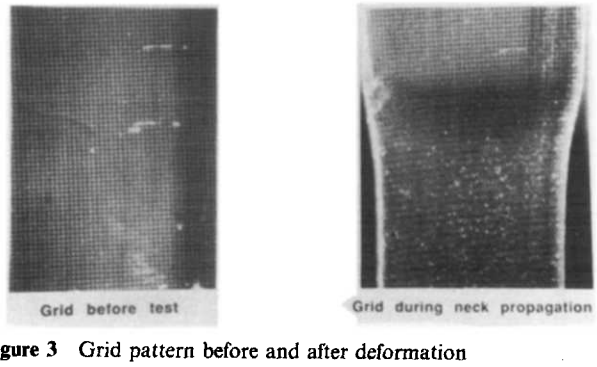

Figure 3 Grid pattern before and after deformation

field determination is approached through the stress-optic method, through an extension of standard photoelasticity. In the literature, such extensions are referred to as photoplasticity, but we choose not to use this term. The loaded, necked specimen was placed in a standard polariscope and the isochromatic fringe pattern was recorded. In interpreting the fringe patterns in terms of

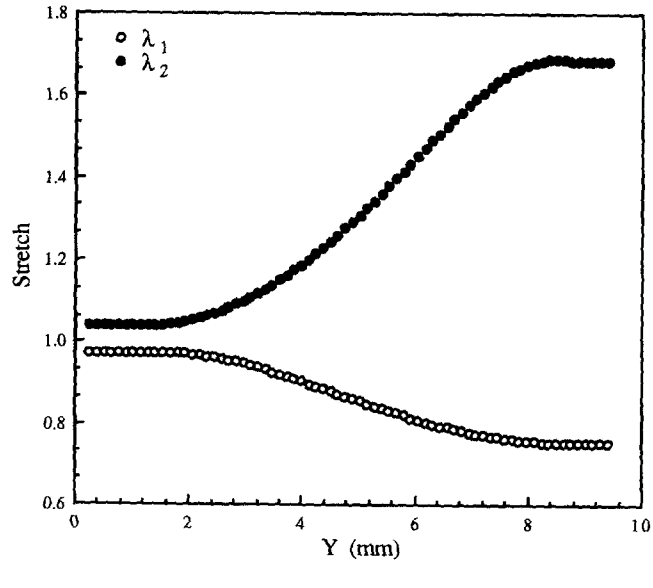

Figure 4 λ_1 and λ_2 (stretches) along the midline at $X = 2.083$ mm

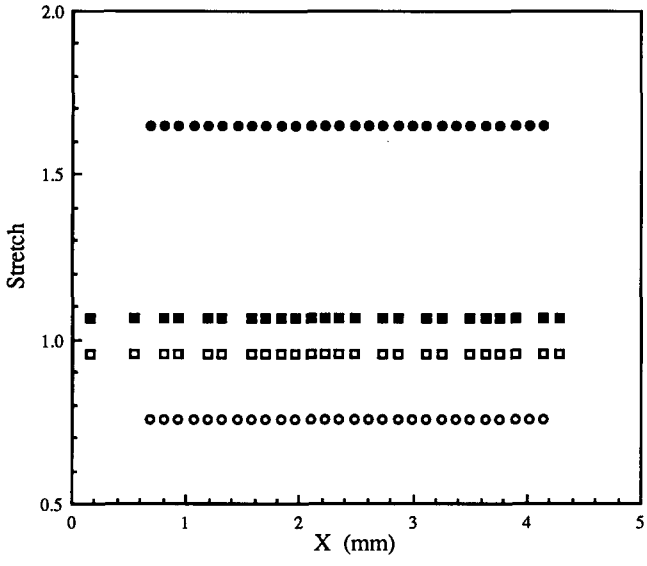

Figure 5 Variation of λ_1 and λ_2 across the specimen at $Y=0.254$ mm (in the elastic region: λ_1 (□), λ_2 (■)) and at $Y=9.271$ mm (in the plastic region: λ_1 (○), λ_2 (●))

the deformation and stress fields, we impose a constitutive assumption and we will first discuss the motivation of this assumption.

Polycarbonate, in the annealed state, is optically isotropic. Upon application of a stress field (under small strain conditions), temporary optical anisotropy (which disappears upon unloading) is introduced, owing to the changes in the molecular polymer chain spacing and orientation. This anisotropy can be observed and measured in a standard polariscope and related to the stress field through standard photoelastic equations. If large irreversible deformations occur, such as in the case of necking and neck propagation, the induced optical anisotropy becomes permanent, owing to the permanent reordering of the molecules. Thus, when the unloaded permanently deformed model is placed in the polariscope, isochromatic fringe patterns are observed; these are due to the permanent deformation. Upon reloading, further temporary optical anisotropy is introduced, owing to the imposed strains, and is superimposed on the permanent patterns. Thus, under conditions of steady-state necking, the induced anisotropy can be decomposed additively into two parts: a temporary component, due to the incremental loading, and a permanent component, due to the inelastic strains. The latter component is sometimes referred as to *form* or *orientation birefringence*. Thus, the stress-optic law relating the optical path difference Δ to the stresses is:

$$N=\frac{\Delta}{2\pi}=C_1h(\sigma_1-\sigma_2)+C_2h(\varepsilon_1^p-\varepsilon_2^p) \qquad (2)$$

where σ_1 and σ_2 are the true principal stresses, ε_1^p and ε_2^p are the inelastic strains and h is the current thickness. This form of the stress-optic law was suggested by Coker and Filon[6]. The constants C_1 and C_2 are obtained from calibration, as discussed below.

The constant C_1 (in the elastic region) was obtained using the standard four-point bend test, whereas, for the determination of the constant C_2, we used the results obtained from the strain analysis. Although the value of C_1 for polycarbonate can be found in technical literature, we felt the need to calibrate our material before and after generating molecular orientation. The calibration was performed on a beam in the annealed state and on a beam stretched to the full draw ratio of ≈ 1.7. The fringe constant $f_\sigma=1/C_1$ was found to be $f_{\sigma_E}=7.6$ kPa m/fringe for the annealed material and $f_{\sigma_0}=8.0$ kPa m/fringe for the fully oriented material. In the case of the oriented material, the birefringence was measured after eliminating the contribution due to orientation. These values are close to the value of 7.5 kPa m/fringe reported in the literature[7].

The constant C_2 was determined using the experiments on the necked specimen. In the unnecked and fully necked regions, σ_1 can be calculated as the load per current area. It should be noted that the triaxiality factor in these regions is unity. Also, the permanent strains developed between the fully necked and the unnecked points is known from the strain measurements. If the fringe numbers at these two points are obtained experimentally, then C_2 could be calculated using equation (2). Furthermore, once C_2 is determined (equation (2)), along with measurements of the strains and fringe variation along the neck, the stress field $(\sigma_1-\sigma_2)$ along the neck can be obtained.

When the loaded, necked specimen is placed in a standard polariscope, the light rays, generated from a helium–neon laser, refract in the region where necking occurs, due to the change in thickness of the specimen; therefore, the fringes could be seen only in the regions where the material was elastically deformed or fully oriented but not in the transition zone, as shown on the left-hand side of *Figure 6*. Brinson[8] reported the same problem when studying the viscoelastic–plastic behaviour of polycarbonate under uniaxial loading. To overcome the problem of the light refracted due to the deformations, the specimen was placed in a transparent tank containing a liquid (mixture of different types of oil) with an index of refraction close to that of polycarbonate. Therefore, when the light rays entered the specimen in the highly deformed region, the refraction was greatly reduced; a continuous fringe pattern could be observed from the elastic region up to the fully oriented region. This is shown in the middle section of *Figure 6*. Because of the very high fringe density (around 100 fringes/mm in the middle of the necked region), a microscope was used to resolve the fringes. The fringe pattern was then recorded from the elastic region down to the fully extended zone using a Nikon camera coupled to the microscope. The camera and microscope were mounted on a screw-driven

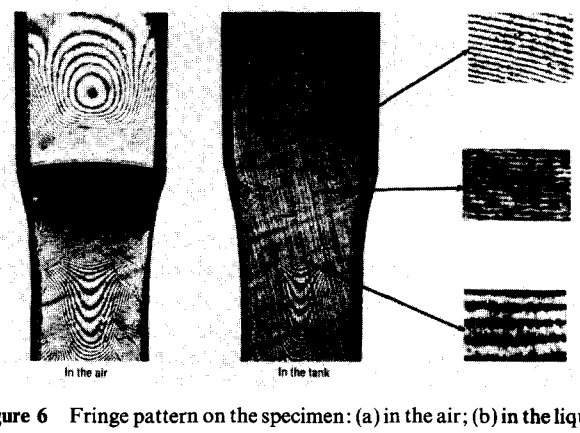

Figure 6 Fringe pattern on the specimen: (a) in the air; (b) in the liquid

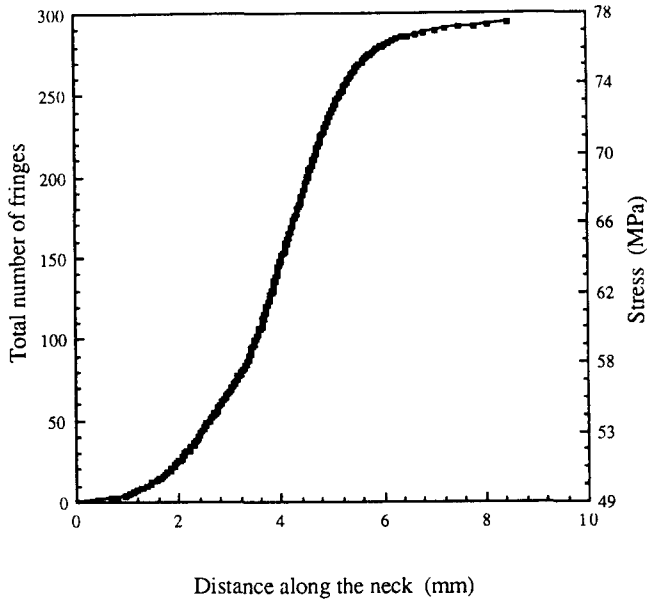

Figure 7 Tensile stress variation along the neck

device in order to record precisely the fringe pattern in the necked region. Thus, the complete fringe pattern from the unnecked to fully necked region was obtained. The variation of fringe number with position along the neck is shown in *Figure 7*. This can now be used to obtain the true-stress–strain relationship.

TRUE-STRESS–STRETCH RELATIONSHIP FOR POLYCARBONATE

Once the constants C_1 and C_2 have been determined, the variation of $\sigma_1-\sigma_2$ along the neck is obtained using equation (2) and is shown in *Figure 7*. In the uniform regions, σ_2 is zero; in the neck, results of Tugcu and Neale suggest a very small triaxiality. Thus if we assume that σ_2 is negligible all along the neck, then *Figure 7* can be considered to be the variation of true stress σ_1 along the neck.

Hence for every point located along the midline of the specimen, the state of stress and strain can be determined. Correlating these two results, a plot of the stress–stretch curve for stretches in the range of 1 to 1.7 can be obtained as shown in *Figure 8*. On this graph, two different curves are plotted:

(i) stress–stretch behaviour before necking, obtained simply from the load–elongation plot shown in *Figure 2*; and

(ii) stress–stretch behaviour once the neck propagates under steady-state conditions, obtained using the detailed stress and strain measurements.

A corresponding representation in strain space is shown in *Figure 9*. Thus when the applied load is increased, the material goes from the unloaded state (point A) to the stressed state (point B), where the necking instability occurs, corresponding to the peak load. The nature of the instability initiating necking depends on the geometry of the specimens. In square and rectangular cross-sections, triaxiality is reduced and thus the shear instability predominates; Lüder's bands appear as shown inset in *Figure 2*. In round bars, the instability initiates either as an axisymmetric neck profile directly at a much higher load than the square sections or in some cases forms Lüder's bands and then develops the necked profile. In either case, the localization spreads into a steady-state neck propagation at constant load. This localization in the deformation results in a partial unloading of the material away from the neck region. These points in the material will therefore unload and go from point B to point C on the stretch–stress curve. Since the load remains constant during the growth or propagation of the neck, the material stays at the same stress–strain state (point C) until the neck reaches that region. At that instant, under the deformations induced by the neck, the material will start to behave along another path in the strain space as well as another stress–stretch path (from point C to point E) corresponding to generation of molecular orientation and the beginning of the tightening of the entanglement of the molecular chains in that region.

For the point in the material where deformation localization occurs, the strain path remains similar to the one previously described (up to point B). At that point and location on the specimen, if some kind of defect is present, the shear bands form. Since we know the path

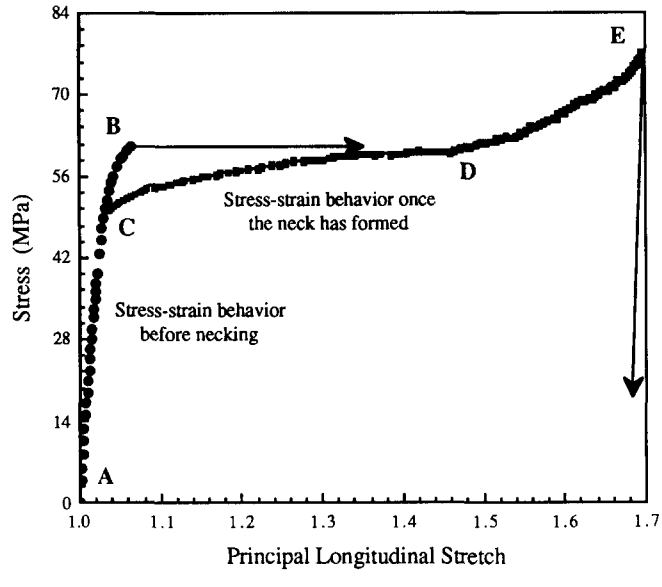

Figure 8 Stress–stretch behaviour of polycarbonate

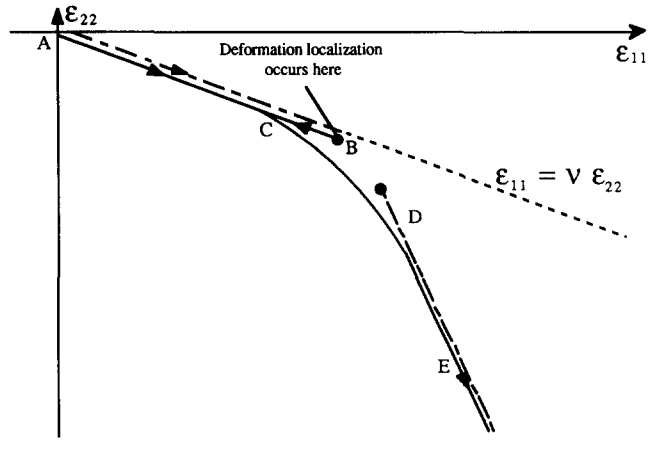

Figure 9 Strain space representation: strain paths for a particle when the neck first forms (----) and once the neck has formed (——)

followed in the first case by the same material up to full orientation, we know that both should behave in a similar way at large strains. During the formation and stabilization of the shear bands, i.e. from point B to D on the stress–stretch curve, the actual stress–strain path taken by the material initiating localization is undetermined. The unloading of the new material formed by the orientation is still elastic but with a different slope, since the modulus of elasticity of the oriented material is higher. Generalization of this uniaxial characterization to the multiaxial loading situation would require more extensive experiments. In the present example, it is possible to follow the fringe patterns along other lines parallel to the specimen midline; along these lines, the stress and strain states are multiaxial. However, interpretation of the data would be much more complicated than the one illustrated here and is therefore not attempted. Also, generalization of the yield criterion to multiaxial states would be required. An alternative approach would be to consider the material to be non-linearly elastic (without unloading) and use an elastic potential such as the Odgen potential.

CONCLUSIONS

It has been demonstrated that, through a detailed characterization of the stress and strain variation along the neck, the true-stress–stretch characterization can be obtained. While the same technique can be used for multiaxial loading conditions, the associated problems are more complex.

REFERENCES

1 Hutchinson, J. W. and Neale, K. W. *J. Mech. Phys. Solids* 1983, **31**, 405
2 Tugcu, P. and Neale, K. W. *J. Mech. Phys. Solids* 1985, **33**, 323
3 Tugcu, P. and Neale, K. W. *Int. J. Solids Struct.* 1987, **23**, 1063
4 Stokes, V. J. and Nied, H. F. Proc. Symp. on Constitutive Modeling for Non-Traditional Materials, ASME, 1987
5 G'Sell, C. and Jonas, J. J. *J. Mater. Sci.* 1979, **14**, 583
6 Coker, E. G. and Filon, L. N. G. 'A Treatise on Photoelasticity', Cambridge University Press, Cambridge, 1957
7 Kuske, A. and Robertson, G. 'Photoelastic Stress Analysis', Wiley, New York, 1974
8 Brinson, H. F. in 'Deformation and Fracture of High Polymers', (Eds. Kaush *et al.*), Plenum Press, New York, 1972